Title

Human tear-production rate from closed-eye Schirmer-strip capillary dynamics

Authors

Telles, R
Li, W
Dursch, TJ
et al.

Publication Date

2017-05-01

DOI

10.1016/j.colsurfa.2016.08.027

Peer reviewed

Human tear-production rate from closed-eye Schirmer-strip capillary dynamics

R. Telles[a], W. Li[b], T.J. Dursch[a,b], M.C. Lin[b,c], C.J. Radke[a,c,*]

[a] Chemical and Biomolecular Engineering Department, University of California, Berkeley, CA, 94720, United States [b] Clinical Research Center, School of Optometry, University of California, Berkeley, CA, 94720, United States [c] Vision Science Group, University of California, Berkeley, CA, 94720, United States

∗ Corresponding author at: Department of Chemical and Biomolecular Engineering, University of California, Berkeley, 101E Gilman Hall, Berkeley, CA, 94720−1462, United States. E-mail address: radke@berkeley.edu (C.J. Radke).

Graphical Abstract

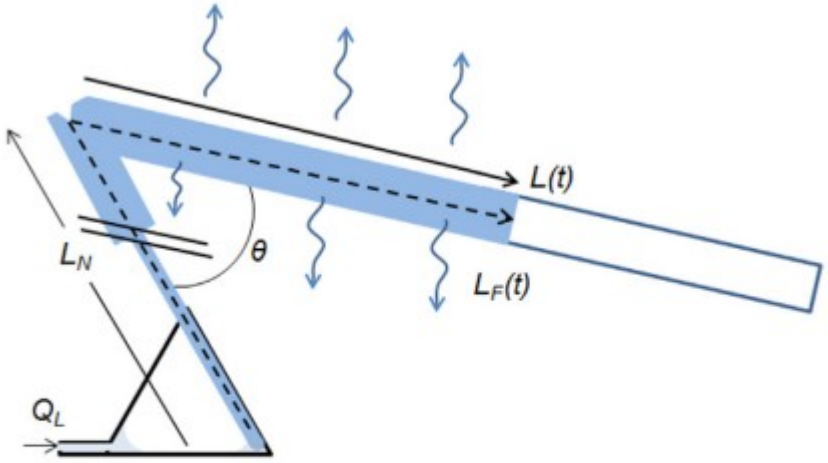

Schematic of a Schirmer strip inserted into the tear prism of the lower fornix of a closed human eye. Wetted strip is colored. Curved lines with arrows indicate tear evaporation Dark parallel lines indicate a size-scale change. Drawing is not to scale.

Abstract

A Schirmer tear test (STT) is commonly used to gauge human tear production, especially when dry-eye symptoms present. In an STT, the rounded tip of a standardized paper strip is inserted into the lower fornix of the eye, and the wetted length extending out from the lower lid is recorded after 5 min of eye closure. Longer wetted lengths suggest higher tear production rates. To date, however, there is no methodology to transform STT transient wetting lengths into basal tear- production rates. We develop a physical model to elucidate wetting kinetics in a Schirmer strip. Tear evaporation from the exposed portion of the strip and gravity are accounted

for. Careful consideration of the initial depletion of tear in the closed-eye tear prism reveals an initial fast increase in wetted length followed by slower growth. Excellent agreement of the proposed model is achieved with experimental observation. When evaporation is negligible, the slow-growth regime exhibits a linear increase of wetted length in time. The linear-length-growth time regime permits simple calculation of quantitative tear-production rates. We suggest measuring several dynamic wetting lengths along a sheathed Schirmer strip and near the 5-min insertion duration followed by fitting to a straight line. The slope of the length-versus-time data gives the basal lacrimal-supply rate.

Keywords: Capillary imbibition, Tear evaporation, Human lacrimal-production rate, Schirmer-tear test

1. Introduction

Accurate assessment of tear production is critical to diagnosing eye health. A simple, clinical test for measuring human tear production dates back to Schirmer in 1903 [1]. As now practiced in a Schirmer tear test (STT) [2], a 0.2-mm thick paper strip (Standard Schirmer Tear Test Strip, Whatman standard filter paper # 41, Alcon Laboratories, Fort Worth, TX), 5-mm wide and 35-mm long, is folded at a notch located 5 mm from the rounded end of the strip and gently inserted into the inferior fornix (Table 1 lists pertinent properties of a standard Schirmer strip [2–15]). After 5 min of eye closure, or until the patient's tear fills the entire strip, the Schirmer strip is removed, and the wetted length beyond the notchis recorded [2]. Tear productionis classified as "normal" when the wetted length is more than 10 mm, as "deficient" or "dry eye" if less than 5 mm [2,16,17], and "equivocal" when lying between 5 and 10 mm. Translation of STT wetting lengths into quantitative tear-production rates, for example in μL/min, presents several challenges. First, physical insertion of the strip initiates reflex tearing and irreproducibility, both of which cloud assessment of basal tear production [18]. Local anesthesia improves reproducibility of the measurement [2]. Fig. 1 shows an average of STT wetted lengths and variability for 50 subjects under local anesthetic [18]. Here, all subjects' lacrimal production is healthy according to STT. Second, evaporation of tear from the strip into the environment slows liquid penetration [19] and adds to variability unless evaporation is prevented [19]. We find that a simple analysis to obtain lacrimal-production rate is precluded when evaporation cannot be neglected.

Even though STT has been used for over one hundred years as a common clinical test to diagnose dry eye, physical underpinnings are poorly understood [19–26]. To provide clinicians with insight into whatis actually measured [18–30], itis essentialto understand the physical foundations of STT. Elucidation of the wetting kinetics in a Schirmer strip is particularly important when attempting to obtain quantitative lacrimal-production rates.

Holly and coworkers [19,22–24] were apparently the first to evaluate volumetric tear-production rates, Q_L, from STT. These authors observed that

the wetting length increases rapidly at short times but slows at longer times. Fig. 2 for canine eyes illustrates the effect [25]. At first, wetting length extends rapidly, followed by a slower, approximately linear increase in time. Holly and colleagues argue that the initial fast-time regime is due to reflex tearing that later slows exponentially to a normal basal rate [19,22–24]. Unfortunately, Holly's picture leads to an exponential approach in time of the wetted length to a final constant value, and, thus, only approximates measured behavior in Figs. 1 and 2. A pivotal assumption of Holly et al. [19,22–24] is that lacrimal production directly supplies the Schirmer strip (so-called limited supply) with no influence of capillary suction [19,22–24]. Capillary-driven wicking [31,32] by a Schirmer strip occurs faster than does lacrimal supply. However, from the Young-Laplace [33,34] and Darcy laws [15,32,35], wicking wetted length scales as the square root of time [19,32–34]. It is not straightforward to explain the measured linear time dependence of penetration lengths seen in Figs. 1 and 2.

This work presents a physical model to describe selfconsistently the observed kinetics of liquid wetting of an inserted Schirmer strip including evaporation and gravity. We investigate conditions necessary for measured wetting lengths to be linear in time and whether quantitative lacrimal volumetric-production rates may be ascertained. Numerical evaluation of the proposed physical model captures the wetting kinetics in a porous paper strip.We then apply model results towards measuring reliable tearproduction rates. Our effortis based on the extensive work of Starov on wetting dynamics [32]. By explicitly accounting for capillary suction from the closed-eye tear lake into the Schirmer strip, we expose three time regimes. First, the strip very quickly depletes tear swept into the tear lake during eye closure. Depletion local to the inserted strip, however, is not complete. Very small arc menisci remain in the corners of the tear prism with small radii of curvature that almost match the menisci curvature in the Schirmer strip. Thereafter, in the second time regime, tear penetration into the strip dramatically slows because the curvature-induced-driving pressure difference approaches zero. Consequently, in the second time period, tear-lake menisci adjacent to the strip establish nearly constant curvature; lacrimal supply then dominates flow into the Schirmer strip. Since the wetting front emerges from the fornix slightly before the second time regime, tear evaporation further slows progression of the wetted length depending on the rate of tear evaporation relative to that of lacrimal production. Gravity, conversely, enhances front progression. If evaporation is precluded [20,23,25], a linear time-dependent wetting length arises in regime 2. A third time period appears when the strip hydrodynamic resistance to imbibition increases enough at longer wetting lengths that lacrimal supply refills the tear lake. This third time period, however, is beyond the time scale of clinical experiment. Our analysis of Schirmer-strip dynamics including evaporation and gravity predicts exponential-length imbibition dynamics in the second and longest time regime. When

evaporation is minimal, linear-length imbibition dynamics emerges. There is no need to invoke transient decay of reflex-induced tear supply to explain the observed kinetic slowing of the Schirmer-strip wetted length.

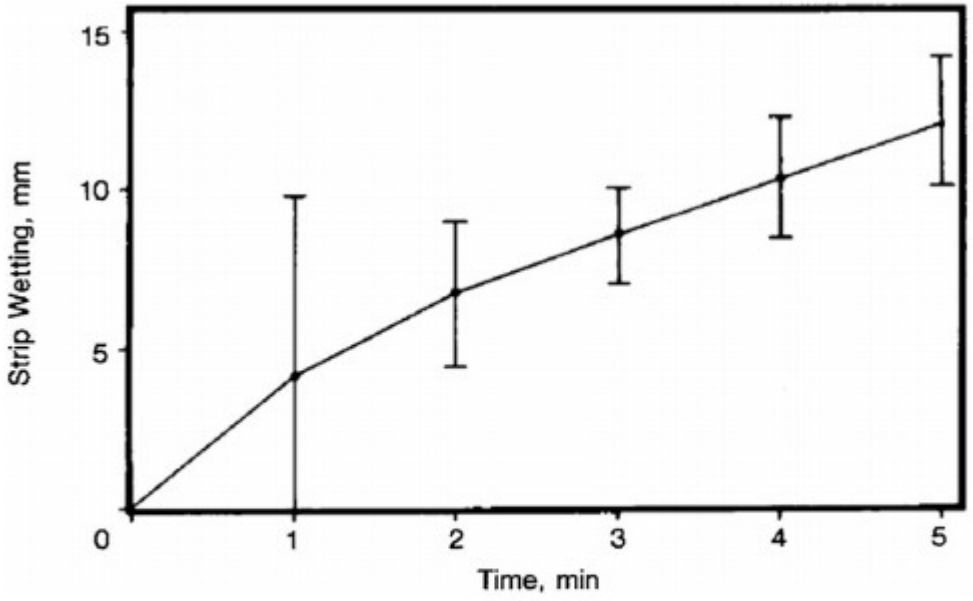

Fig. 1. Schirmer-strip average wetted length and standard deviation for 50 human subjects under local anesthetic as a function of time. Solid line connects datum points. (From Clinch et al. [18] with permission).

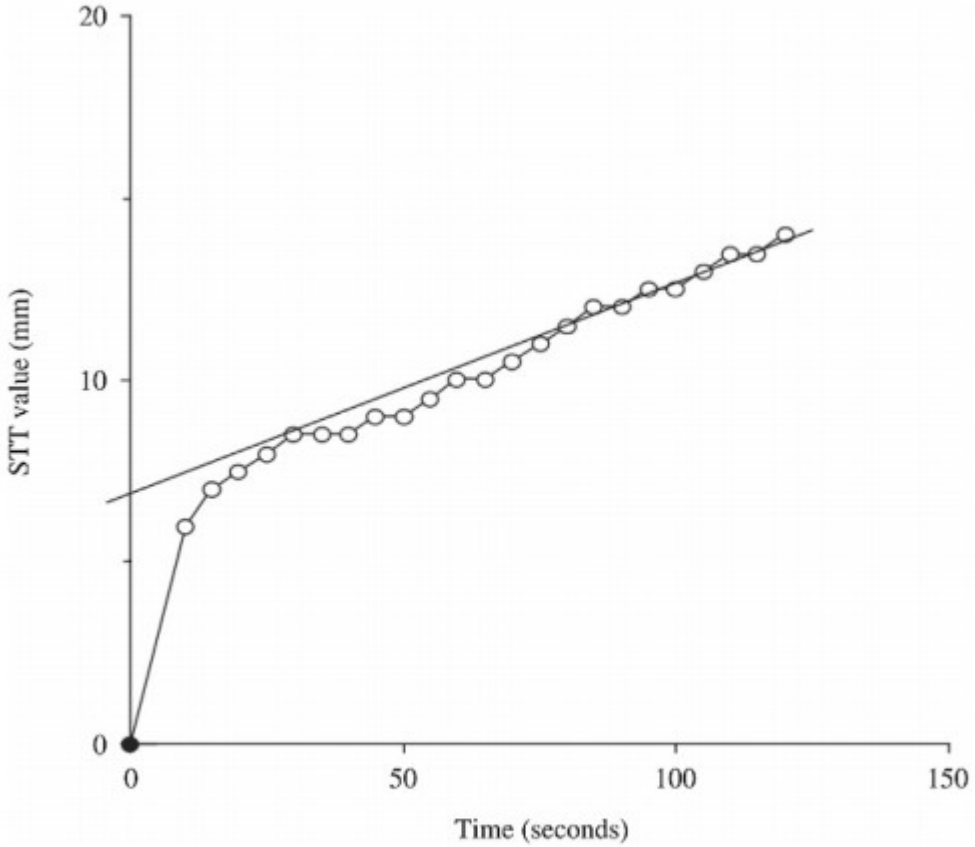

Fig. 2. Schirmer-strip uptake length in a normal canine eye (open symbols). Solid line illustrates linear regression in the last 1 min of test (from Williams with permission [25]).

Table 1
Physical Parameters of Schirmer Strip and Closed-Eye Tear Prism.

Parameter	Symbol	Value (common)	(SI units)	Source(s)
Tear surface tension	γ	45 mN/m	0.045 N/m	[3]
Tear viscosity	μ	1.5 cP	0.0015Pa · s	[4]
Lid-margin perimeter	λ	30 mm	0.03 m	[5]
Blink-filled tear-lake volume	V_{BF}	2.5 μL	2.5×10^{-9} m^3	[6–8]
Tear-lake inscribed radius	R_{ins}	0.233 mm	2.33×10^{-4} m	Calculated
Tear-lake height	h_{TL}	0.70 mm	7.0×10^{-4} m	[9]
Tear-lake side length	L_{TL}	0.81 mm	8.1×10^{-4} m	Calculated
Tear-lake volume	V_{TL}	8.5 μL	8.5×10^{-9} m^3	Calculated
Schirmer-strip porosity	ϕ	0.7	0.7	[10–12]
Schirmer-strip thickness	δ	0.2 mm	2.2×10^{-4} m	[2,13]
Schirmer-strip width	w	5 mm	5×10^{-3} m	[2,13]
Schirmer-strip pore size	R_p	11 μm	1.1×10^{-5} m	[2,13]
*Schirmer-strip permeability	κ	0.41 μm^2	4.1×10^{-13} m^2	[10,13,14]
Schirmer-strip notch length	L_N	5 mm	5.0×10^{-3} m	[2]

* From measured Herzberg filtration time of 54 s [10,13,14]. Also, pore-size-squared scaling of the Carman-Kozeny expression [15] from the measured permeability ($\kappa = 0.062$ μm^2 [10]) and pore radius ($R_p = 4$ μm [10,13,14]) of Whatman 40 filter paper gives a value of 0.45 μm^2.

2. Physical model

Figs. 3 and 4 illustrate lacrimal supply to the inferior tear-lake prism during closed eye following Schirmer-strip insertion. As the superior eyelid closes after strip insertion, tear film and upper and lower-lid tearmenisci are swept into the tear-lake prism. For ease of analysis, the tear-prism cross section is

approximated as an equilateral triangle with an apex height, h_{TL}, located at the gray line (i.e., at the wetting transition [9]), about 0.7 mm above the cornea [9]. For a tear-prism margin of about 30 mm [9], approximately 2–3 μL of tear are gathered into the prism after each blink [7–9]. Anterior-eye anatomy and physiology are outlined elsewhere [9].

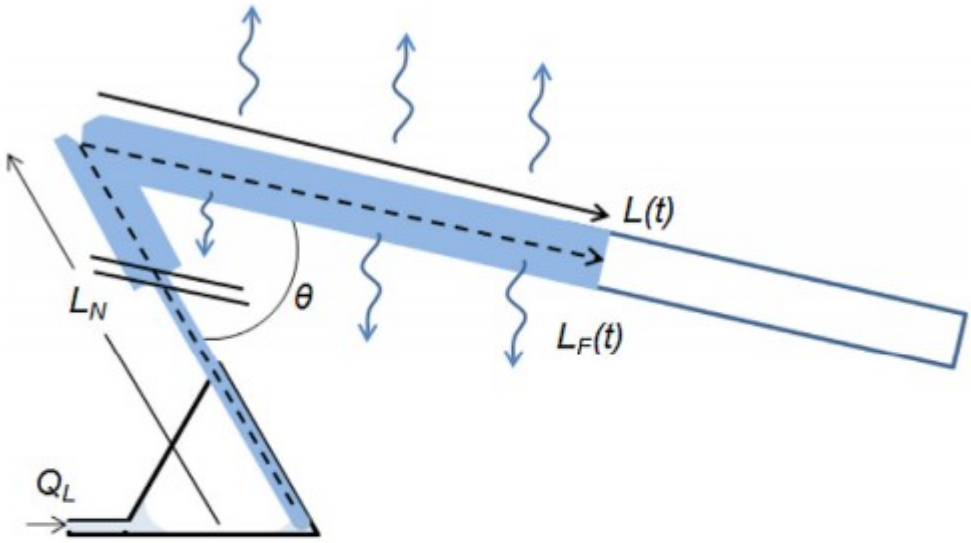

Fig. 3. Schematic of a Schirmer strip inserted into the tear lake shown in cross section as an equilateral triangle that extends a distance λ = 30 mm out of the plane of the paper. Curved lines with arrows indicate tear evaporation. Two dark parallel lines indicate a size-scale change. L_F is the distance from the tear-prism corner to the invading front, shown dashed. L_N is the distance from the tear-prism corner to the strip notch, and L is the clinically measured distance from the notch to the invading liquid front. The exposed portion of the strip makes an angle θ with vertical. Drawing is not to scale.

Some of the initial-collected tear along with tear from the papebral and bulbar conjunctiva surfaces immediately soaks into the liquid-contacted portion ofthe inserted strip. Figs. 3 and 4 illustrate that remaining blink-swepttear over thatinitially absorbed resides in the arc menisci of the tear prism. In Figs. 3 and 4, we attribute the remaining tear-prism liquid volume to that in the corners. As illustrated in Fig. 3, creasing of the Schirmer strip at the notch sets an angle θ with the vertical. θ is taken as constant at approximately 20°.

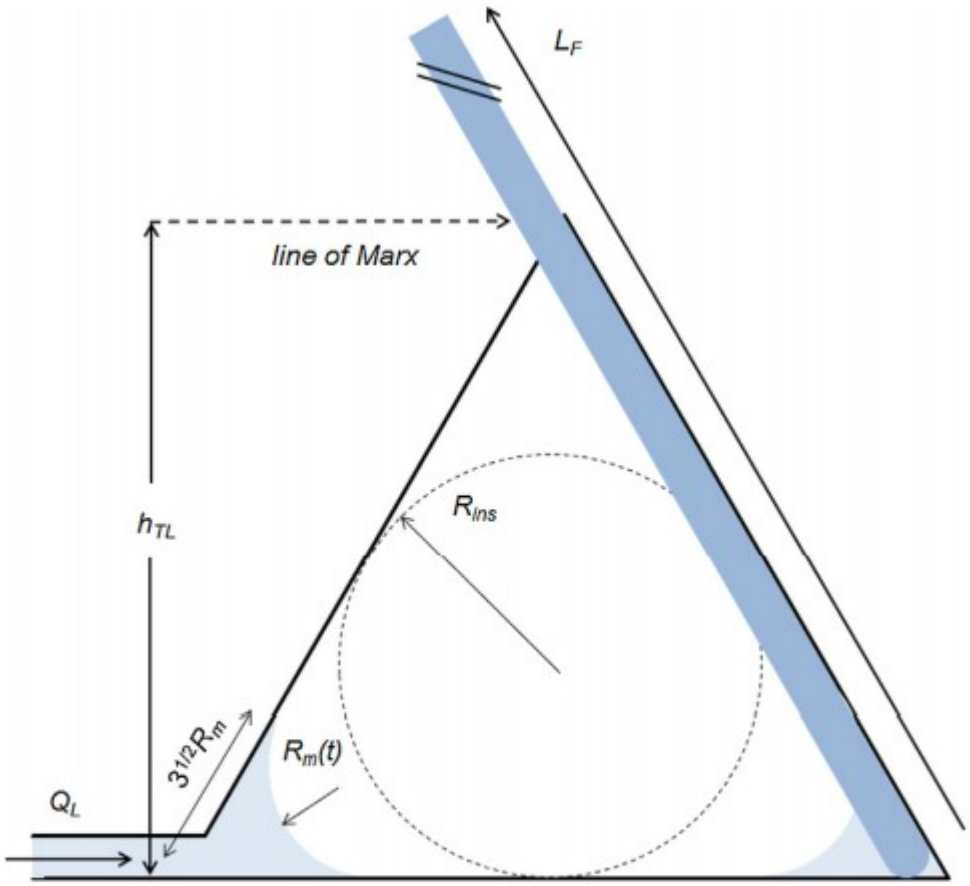

Fig. 4. Expanded cross-section schematic of the tear prism accentuating the arc menisci and inserted strip in Fig. 3. The tear-lake extends a distance $\lambda = 30$ mm out of the plane of the paper. Two parallel lines correspond to those in Fig. 2 and indicate a size-scale change. Tear-lake cross-section size is scaled by the inscribed circle of radius R_{ins}. Distance from the cornea to the gray lines is $h_{TL} \sim 0.7$mm [9]. Transient corner-menisci radius is $R_m(t)$. Drawing is not to scale.

Tear in the arc menisci is the source for impregnating the Schirmer strip. Lacrimal glands supply tear to the superior and inferior 30-mm long cylindrical corner menisci at volumetric production rate, Q_L. These, in turn, feed the 5-mm wide strip. Compared to the flow resistance in the strip, we invoke unhindered lateral flow along the cylindrical arc menisci. As sketched in Fig. 3,tear evaporation commences from both the top and bottom of the strip once the wetted portion of the strip emerges from the inferior fornix. Evaporation slows progression of the wetting front, whereas gravity increases that progression.

Holly et al. [19,22–24] invoke a reflex-induced lacrimal supply that at first is large but then settles to a constant normal rate. In our current analysis, Q_L is constant. Conversely, tear volumetric flow rate into the Schirmer strip, $Q_S(t)$, is a strong function of time.

For constant liquid density, mass conservation of liquid in the arc menisci reads

$$\frac{dV_{AM}}{dt} = Q_L - Q_S(t) \text{ corner menisci} \quad (1)$$

where V_{AM} is the volume of tear in the corner arc menisci (see Figs. 3 and 4). In Eq. (1), we neglect possible lacrimal flow into expanding fornixes upon continuing eye closure [8]. Geometry gives the tear volume in the two arc menisci

$$V_{AM} = 2(\sqrt{3} - \pi/3)R_m^2\lambda = 1.370R_m^2\lambda \quad (2)$$

where λ is the length of the lid margin [7,9] and R_m is the transient arc-menisci radius in the tear prism defined in Fig. 4. Table 1 gives typical anatomical dimensions of the tear lake [9].

Likewise, mass conservation in the Schirmer strip demands that

$$\phi w\delta \frac{dL_F}{dt} = Q_S(\mathrm{t}) \text{ for } L_F < L_N \quad (3a)$$

and

$$\phi w\delta \frac{dL_F}{dt} = Q_S - \frac{2\hat{J}_E\varphi w}{\hat{\rho}}(L_F - L_N) \text{ for } L_F \geq L_N \quad (3b)$$

where w is the width and δ is the thickness of the Schirmer strip, respectively (i.e., $w\delta$ is the Schirmer-strip channel cross-section area), ϕ is the porosity of the paper strip, $\hat{\rho}$ is the mass density of tear, and $\hat{J}_E$ is the evaporation flux of tear from each side of the strip (i.e., mass loss per unit time per unit exposed strip area). The second term on the right of Eq. (3b) accounts for evaporation from both sides of the Schirmer strip (i.e., giving rise to the factor of 2). Evaporation does not occur until the wetting front reaches the strip notch and increases as the wetted length increases. As shown by the dashed line in Fig. 3, L_F is the distance from the rounded end of the inserted strip to the dynamic wetting front. After the imbibition tear front reaches the strip notch, $L_F(t) = L_N + L(t)$, where L_N is the distance between the strip notch and the rounded end of the strip (i.e., 5 mm) and L is the clinically measured wetted-front distance.

Evaporation of tear (taken as that of pure water) from the Schirmer strip is mass-transfer controlled [15,35–37] or

$$\hat{J}_E = k_m M_w \left[\frac{P_w^{sat}(T_S)}{R_G T_S} - R_H \frac{P_w^{sat}(T_\infty)}{R_G T_\infty} \right] \quad (4)$$

where k_m is the mass transfer coefficient, M_w is the molar mass of water, R_G is the ideal gas constant, R_H is ambient relative humidity, and $P_w^{sat}(T)$ is the saturation vapor pressure of water at temperature T. Wet-bulb temperature of the strip is T_S, and ambient temperature is T_∞. Appendix A outlines calculation of the strip wet-bulb temperature for a given ambient relative humidity and ambient temperature of 23 °C.

To quantify tear uptake into the Schirmer strip, we treat the paper strip as a fibrous porous medium [10,14]. Darcy's law describing flow in a porous medium reads [15,32,35]

$$Q_S = w\delta\frac{\kappa}{\mu}\frac{\Delta P}{[L_F(t)-\sqrt{3}R_m(t)]} \text{ for } L_F < L_N \qquad (5a)$$

And

$$Q_S = w\delta\frac{\kappa}{\mu}\frac{[\Delta P + \Delta\hat{\rho}g\cos\theta(L_F - L_N)]}{[L_F(t)-\sqrt{3}R_m(t)]} \text{ for } L_F \geq L_N \qquad (5b)$$

where μ is tear viscosity, κ is the hydraulic permeability of the Schirmer strip, $\Delta\hat{\rho}$ is the mass-density difference between tear and air, and g is acceleration of gravity. The arc-menisci-radius correction to the wetted-strip length in the denominator of Eq. (5) accounts for the changing wetted-flow length as the arc menisci recede into (or much later expand from) the prism corners. As arcmenisci recede into the corners of tear lake, R_m decreases, thereby increasing the wetted length over which the suction pressure acts: $L_F(t)-\sqrt{3}R_m(t)$. Gravity proves negligible compared to imbibition curvature forces before the penetration front reaches the notch. However, after the advancing liquid front reaches the notch in Eq. (5b), gravity contributes to the penetration kinetics. Fluid inertia in the strip is neglected.

ΔP in Eq. (5) represents the imbibition-suction pressure difference equal to the liquid pressure in the arc menisci of the tear prism, P_M, minus that of the wetting front, P_L. Arc-menisci liquid pressure, $P_M(t)$ is that at the three-phase contact line. Upon assuming complete water-wetting of both the Schirmer-strip and the palpebral conjunctiva below the wetting lines of Marx [9], the imbibition pressure difference is given by Young-Laplace [32–34]

$$\Delta P = P_M(t) - P_L = \gamma\left(\frac{2}{R_p} - \frac{1}{R_m(t)}\right) \qquad (6)$$

where R_p is the average pore radius of the fibrous porous strip. Absence of a factor of 2 for the arc-menisci curvature in Eq.(6) arises because tear-lake menisci are cylindrical. As tear in the arc menisci imbibes into the Schirmer strip, the menisci radius R_m decreases. Accordingly, Eq. (6) predicts a smaller

pressure difference for liquid suction into the Schirmer strip. This observation explains the slowing of the strip-uptake rate seen in Figs. 1 and 2.

Eqs. (1)–(6) lead to two, coupled ordinary differential equations to specify the arc-menisci radius, $R_m(t)$, and the wetted length of the Schirmer strip, $L_F(t)$.

$$\frac{dR_m}{dt} = \frac{1}{2.74\lambda R_m(t)}\left[Q_L - \frac{2\omega\delta\gamma\kappa}{\mu R_p}\frac{[1-0.5R_p/R_m(t)]}{[L_F(t)-\sqrt{3}R_m(t)]}\right], \tag{7}$$

$$\frac{dL_F}{dt} = \frac{2\gamma\kappa}{\phi\mu R_p}\frac{[1-0.5R_p/R_m(t)]}{[L_F(t)-\sqrt{3}R_m(t)]} \text{ for } L_F < L_N \tag{8a}$$

and

$$\frac{dL_F}{dt} = \frac{2\gamma\kappa}{\phi\mu R_p}\frac{[1-0.5R_p/R_m(t)]}{[L_F(t)-\sqrt{3}R_m(t)]} + \frac{\Delta\hat{\rho}g\kappa\cos\beta}{\phi\mu}\frac{[L_F(t)-L_N]}{[L_F(t)-\sqrt{3}R_m(t)]} - \frac{2\hat{J}_E}{\delta\hat{\rho}}(L_F - L_N) \text{ for } L_F \geq L_N \tag{8b}$$

Initial conditions for Eqs. (7) and (8) depend on the volume of tear in the tear lake immediately after insertion of the Schirmer strip. We assume that the initial arc-menisci radius is close to that of the inscribed radius of the tear prism

$$R_m(0) = R_{ins} \tag{9}$$

Since $R_{ins} = h_{TL}/3 = 0.233$ mm, Eq. (2) sets the initial tear volume in the arc menisci as 2.25 μL, close to that swept into the tear lake after a blink. In addition, the portion of the strip manually inserted into the inferior fornix gathers tear immediately from the papebral conjunctiva and partially from the bulbar conjunctiva. Thus, most of the Schirmer strip below the notch is wetted prior to commencement of wicking. Therefore, we set the initial wetted length as

$$L_F(0) = \beta L_N \tag{10}$$

where β is a constant, close to unity, specifying the fraction of the strip that is pre-wet during insertion. As demonstrated below, details ofthe initial conditions do notimpact clinically measureable wetting dynamics in the STT.

To enhance physical understanding, we recast the governing equations in dimensionless form. Let

$$R = R_m/R_{ins};\ \Lambda_F = L_F/R_{ins}; \text{and } \tau = \frac{Q_L}{2.74\lambda R_{ins}^2}t \tag{11}$$

Substitution of these definitions into Eqs. (7) and (8) gives

$$\frac{1}{2}\frac{dR^2}{d\tau} = \left[1 - \alpha\frac{(1-\rho/R)}{\left(\Lambda_F - \sqrt{3}R\right)}\right], \tag{12}$$

$$\frac{d\Lambda_F}{d\tau} = \nu\frac{(1-\rho/R)}{\left(\Lambda_F - \sqrt{3}R\right)} \quad \text{for}\,\Lambda_F < \Lambda_N\,, \tag{13a}$$

and

$$\frac{d\Lambda_F}{d\tau} = \nu\frac{(1-\rho/R)}{\left(\Lambda_F - \sqrt{3}R\right)} + G\frac{(\Lambda_F - \Lambda_N)}{\left(\Lambda_F - \sqrt{3}R\right)} - E(\Lambda_F - \Lambda_N)\ \text{for}\ \Lambda_F \geq \Lambda_N \tag{13b}$$

where

$$\alpha = \frac{2\gamma w\delta\kappa}{\mu Q_L R_p R_{ins}};\ \nu = 5.48\frac{\gamma\lambda\kappa}{\phi\mu Q_L R_P};\ \rho = 0.5R_P/R_{ins};$$

$$E = \frac{5.48\lambda R_{ins}}{\delta Q_L}\frac{\hat{J}_E}{\hat{\rho}};\ \text{and}\ G = 2.74\frac{\Delta\hat{\rho}g\lambda\kappa R_{ins}\cos\beta}{\phi\mu Q_L} \tag{14}$$

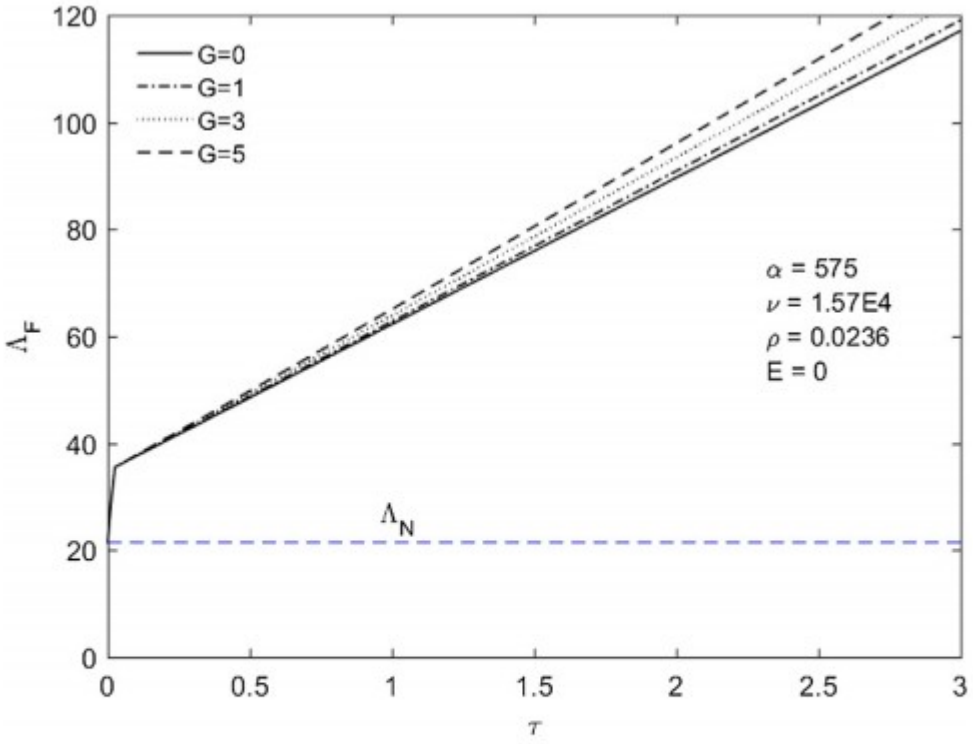

Fig. 5. Reduced wetting length of strip as a function of reduced time for various dimensionless gravity numbers, G. With $\theta = 20^{\circ}$ and Table 1 parameters, $G = 4.13$. Increased gravitation numbers increase rate of tear penetration into the stip. A dashed line indicates dimensionless location of the notch at $\Lambda_N = 21.4$. $Q_L = 1\ \mu L/\min$.

The evaporation number, E, controls the influence of evaporation on strip wetting dynamics while the gravitation number, G, controls the importance of gravity in enhancing imbibition rate. Initial conditions now read

$$R(0) = 1 \text{and} \Lambda_F(0) = \beta \Lambda_N \qquad (15)$$

where $\Lambda_N = L_N/R_{ins} = 21.4$ and we set $\beta = 0.99$. Eqs. (12) and (13) are solved numerically by the stiff differential equation solver, ode15s, in Matlab [Mathworks, Inc. Natick, MA] subjectto the initial conditions in Eq. (15). Table 1 lists necessary parameters. Knowing the wetted-strip length, $L_F(t)$, the clinically measured length, $L(t)$, is easily found by subtracting the inserted distance to the notch, L_N(= 5mm).

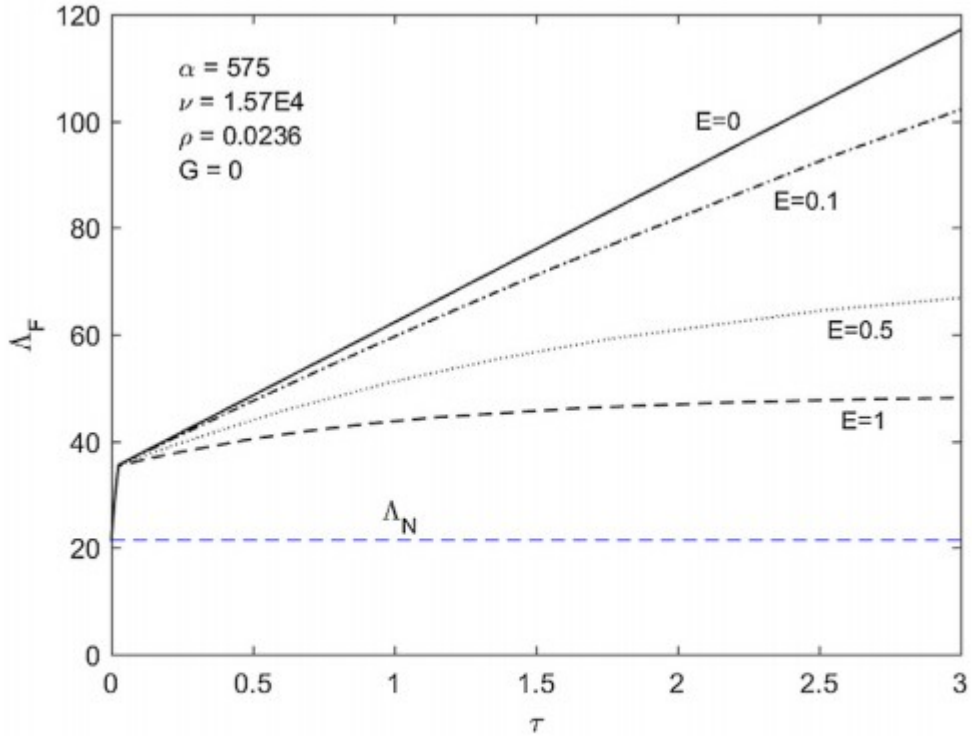

Fig. 6. Reduced wetting length of strip as a function of reduced time for various dimensionless evaporation numbers, *E*. Increased evaporation slows tear penetration into the stip. A dashed line indicates dimensionless location of the notch at $\Lambda_N = 21.4$. $Q_L = 1$ μL/ min.

3. Results

Figs. 5 and 6 explore the roles of gravity and evaporation, respectively, in strip wetting dynamics. Dimensionless total-strip wetting length is plotted as a function of reduced time for gravitation numbers up to 5 with no evaporation (Fig. 5) and for evaporation numbers between zero and unity with zero gravity (Fig. 6). Dimensionless parameters α, ν, and ρ are calculated from the physical constants listed in Table 1 with $\theta = 20°$ and with Q_L set nominally at 1 μL/min. Horizontal dashed lines in Figs. 5 and 6 accentuate the dimensionless location of the strip notch at $\Lambda_N = 21.4$. Before reaching this length, the wetting front resides inside the inferior fornix and is not visible. Both figures reveal a fast early-time imbibition (regime 1) followed by a slower penetration time regime (regime 2). Early-time behavior is not clinically accessible.

Table 2
Calculated Evaporation Number as a Function of Relative Humidity at Ambient. Temperature (23 °C)

R_H (%)	[a] $\hat{J}_E$(g/m^2/s)	[a] T_S (°C)	[a] E
25	0.184	19.9	0.35
50	0.105	20.0	0.20
75	0.027	20.1	0.05

[a] From heat and mass transfer correlations for natural convection in Appendix A.

With zero evaporation in Fig. 5, the second time regime gives essentially linear-length wetting dynamics. Increasing gravitation numbers increase the rate of liquid penetration, as expected. For a Schirmer strip, typical gravitation numbers are about 4 and are insensitive to the strip angle. For $G = 4$, there is approximately a 10% increase in strip-penetration rate over that when gravity is neglected.

Depending on the value of E, Fig. 6 reveals that evaporation can exert a major effect on wetted-length dynamics. Increased E slows tear penetration into the strip, especially at later times. Wetting dynamics in the slow-time regime deviates from linear-length kinetics. For nonzero evaporation numbers, a steady state is reached at long time where tear supply to the strip balances evaporative loss. Table 2 reports evaporation numbers at three relative humidities and at ambient temperature (23 °C). Values are calculated in Appendix A from heat and mass-transfer theory for evaporation by natural convection. Theory values for E lie somewhat below 0.5 depending on environment humidity and reinforce the possible important role for evaporation at low humidity.

Results in Fig. 6 are in general agreement with those of Buckmaster and Pearce, including their in-vivo measured wet-bulb temperature of a Schirmer strip [20]. Williams, however, reports no effect of sheathing Schirmer strips against evaporation for canine eyes [25]. Evaporation rates are not known precisely for a Schirmer strip hinged on a human eyelid. Actual evaporation rates are likely curtailed compared to those from theory for an isolated plate.

Fig. 7 displays corresponding dimensionless arc-menisci radii as a function of dimensionless time for a range of gravity and evaporation numbers. To uncover early-time behavior of the proposed model, a base-ten logarithmic time scale is adopted. As opposed to wetting dynamics, there is no discernable effect of gravity or evaporation on arc-menisci radii kinetics.

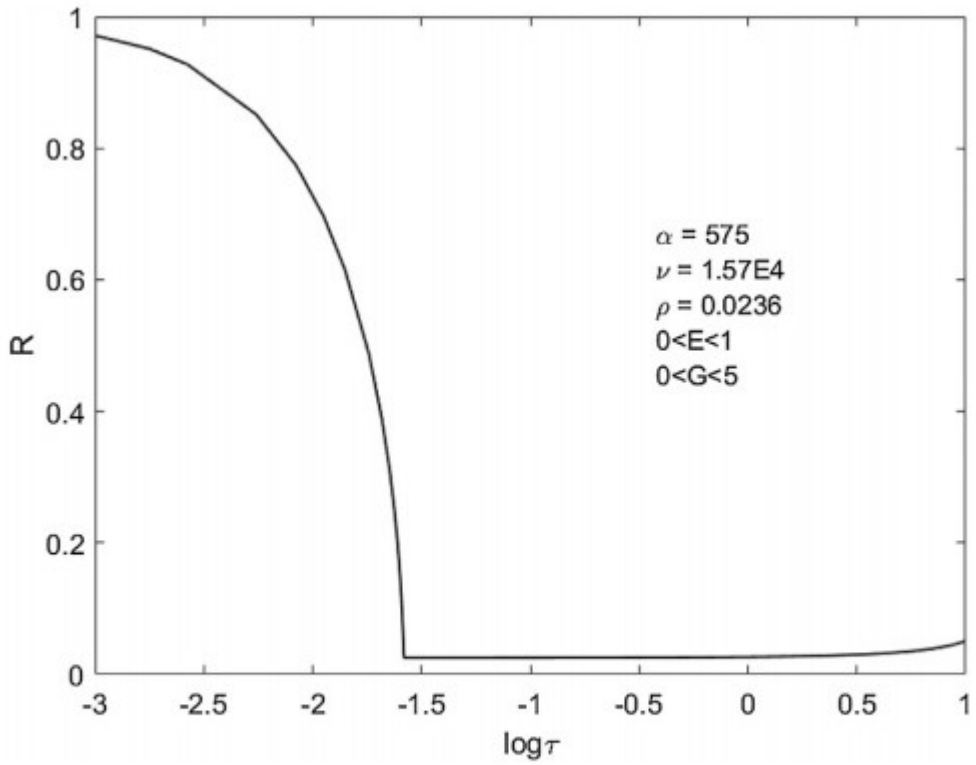

Fig. 7. Reduced arc-menisci radius a function of base-ten logarithmic reduced time. Tear quickly recedes into tear-prism corners until $\tau \sim 0.025$ and slowly increases thereafter. Three time regimes appear: 1. initial decreasing R; 2. nearly constant R; and 3 final increasing R. $\theta = 20^{\circ}$; $Q_L = 1 \mu L/\text{min}$.

Fig. 7 exposes three time regimes. In the fast-time regime for values of reduced time less than about $\tau* = 0.025$, arc-menisci radii diminish very rapidly. The initial time regime is seen as a near step change of wetting length in Figs. 5 and 6. Zero-time evaluation of Eq. (12) near $R \sim 1$ reveals that R^2 decreases linearly in reduced time with a negative slope of magnitude $2[1 - \alpha/\Lambda_F(0)]$. This result provides an estimate of the transition time or $\tau* = \{2[\alpha/\Lambda_F(0) - 1]\}^{-1} = 0.019$ in good agreement with the numerical results in Fig. 7. Thus, duration of the initial fast induction period depends on tear and Schirmer-strip properties and also on the initial filling of the strip up to the notch. In Figs. 5–7, the initial filling fraction is 0.99. Less initial filling of the strip below the notch gives a shorter induction time because the length of the wetting strip is smaller which reduces strip viscous resistance (see Eq. (5)).

Up to the transition time, $\tau*$, tear volumes in the corner menisci quickly deplete because of fast capillary suction into the porous Schirmer strip. From Fig. 7, the transition time corresponds to the corner-menisci radii of curvature diminishing close to those in the Schirmer strip (i.e., to $0.5R_p/R_{ins} =$

0.0236). Accordingly, the suction-driving pressure difference approaches zero in Eq.(6) choking capillary imbibition. Following initial fast wicking in the first time region, Fig. 7 reveals that the arc menisci effectively stay near a constant radius of curvature. Consequently, in the second time regime, only lacrimation supplies the Schirmer strip. Tear production feeds both the strip lengthening wetting front and evaporation into the environment. Eventually, at very long times, the lengthening wetting front evolves an ever increasing hydrodynamic flow resistance; the corner menisci adjacent to the strip eventually begin to fill. This effect is seen at reduced times near 10 in Fig. 7. This third time regime is well beyond clinical measurement times and does not appear in Figs. 5 and 6.

Fig. 8 highlights the first two time regimes for wetting dynamics by graphing the abscissa on two time scales: one at short time confirming the initial fast induction time, $0 < \tau < 0.1$, shown on the upper abscissa and one at longer time corresponding to experimental time, $0 < \tau < 3$, shown on the lower abscissa. Wetting-front dynamics in time-regime 2 is characterized by nearly constant arc-menisci radii or $dR^2/d\tau << 1$. The reason for the near constancy of R^2 is the slow lacrimal supply relative to the capillary-uptake rate of a Schirmer strip. Once the initial high suction rate of the strip reduces the arc-menisci radii adjacent to the strip down to a curvature close to those in the fibrous strip, the two terms on the right of Eq. (7) (or (12)) closely balance or

$$\alpha \frac{(1-\rho/R)}{\left(\Lambda_F - \sqrt{3}R\right)} \sim 1 \quad \text{for } \tau \geq \tau^* \tag{16}$$

Substitution of this result into Eqs. (12) and (13b) explains both the slow change in arc-menisci radius and slowing of the imbibition rate after the initial induction period. In particular, Eq.(13b) beyond $\tau*$ reduces to

$$\frac{d\Lambda_F}{d\tau} + \left[E - \frac{G}{(\Lambda_F - 3\sqrt{R})}\right](\Lambda_F - \Lambda_N) = \frac{\nu}{\alpha} \quad \text{for } \tau \geq \tau^* \tag{17}$$

To obtain a conservative estimate of the importance of gravity, we approximate the ratio $(\Lambda_F - \Lambda_N)/(\Lambda_F - 3\sqrt{R})$ as unity. Integration of Eq. (17) then gives

$$\Lambda_F - \Lambda_N = \frac{(\nu/\alpha + G)}{E}\left[1 - \left(1 - \frac{(\Lambda_F^* - \Lambda_N)E}{(\nu/\alpha + G)}\right)\exp[-E(\tau - \tau^*)]\right]$$

$$\tau \geq \tau^* \tag{18}$$

where Λ_F evaluated at $\tau*$ equals Λ_F^*. Because the induction time is fast, small changes in the initial conditions have no effect on wetting behavior in time-regime 2. That is, on a clinically accessible time scale, the fast initial period

occurs over a step change in wetting length reflecting the almost immediate shrinkage of the arc menisci (see Figs. 5 and 6). Per Eq.(18), slowing of the wetted length beyond the induction time in Fig. 6 is exponential. At long time, Eq. (18) demands a steady wetted length of $\Lambda_N + (\nu/\alpha_{\text{ˌ}} + G)/E$ where tear supply and evaporation rate balance. Fig. 6 is consistent with this demand.

In the limit of small evaporation numbers, Eq. (18) specifies linear-length dynamics for tear penetration into the strip

$$\Lambda_F = \Lambda_F^* + (\nu/\alpha + G)(\tau - \tau^*) \quad \text{for } \tau \geq \tau^*;\ E \ll 1 \qquad (19)$$

No steady wetted length occurs. Rather, lacrimal supply continually increases the wetted length of the Schirmer strip. Linear-length kinetics in Figs. 5, 6 and 8 demands minimal tear evaporation. A constant slope of wetting length versus time forms the basis for clinically determining quantitative lacrimal production rates. For this to occur, however, evaporation must be minimal.

If we accept a reasonable tear-production rate of Q_L = 1 μL/min [6,7,9], the 0.025 dimensionless induction time corresponds to about 6 s in real time. Zero clinical time is difficult to assess precisely since strip insertion is not exactly reproducible. Consequently, a 6-s induction time until establishment of the second slower growth regime is in good agreement with those clinically documented (https://www.youtube.com/ watch?v=SCJ6n41Vmpc; see also Fig. 2).

4. Discussion

Results in Figs. 5–8 confirm the assertion of Williams [25] that Schirmer-strip dynamics consists of two stages: a fast regime where tear initially in the closed-eye tear lake depletes followed by a slow regime in which tear supply limits the imbibition rate. The model-predicted third time regime, where arc menisci refill, lies beyond the 5-min measurement interval of a STT. When evaporation is negligible, the second slower regime exhibits linear-length growth kinetics. As observed in Figs. 5–8, transition between the two regimes is abrupt [25], not exponentially smooth as suggested by Holly [19,22–24]. Our physical model, however, does not confirm the suggestion of Williams that the intercept of the linearlength growth line (see Fig. 2) reflects the initial volume of tear in the tear lake [25].

Linear-length kinetics in Figs. 5, 6 and 8 provides a simple means to garner quantitative tear-production rates. From Eq. (19), the slope in these figures is $d\Lambda_F/d\tau = \nu/\alpha + G$. Rewriting this result in dimensional quantities gives

$$\frac{\Delta L}{\Delta t} = \frac{Q_L}{\phi w \delta} + \frac{\Delta \hat{\rho} g \kappa \cos\theta}{\phi \mu} \qquad (20)$$

Thus, lacrimal volumetric-production rate is available from the measured slope of the wetted-length-versus-time data and the known parameters of a Schirmer strip provided evaporation is insignificant. As an example, the slope of the last three time points in Fig. 1 is about 1.7 mm/min. If gravity is ignored, a tear-production rate of 1.19 μL/min emerges from Eq. (20), an acceptable value [6,7,9]. Conservative correction for gravity in Eq. (20) gives a tearproduction rate of 1.04 μL/min. Including gravity in the estimate of Q_L results in a downward adjustment of about 10%, in agreement with Fig. 5.

To determine quantitative clinical tear-production rates, we suggest that the Schirmer strip be sheathed [20,23,25] or evaporation otherwise precluded. Next, we recommend utilizing Schirmer strips with mm markings and recording at least three wetting lengths at, for example, 3, 4, and 5 min. A best eye-fit gives the linear slope and, hence, a quantitative tear-production rate from Eq. (20). This procedure replaces that of recording a single length datum at 5 min, but is no more time consuming or inconvenient to the subject or clinician.

Our proposed methodology applies only to the linear-length time regime, which is established very soon after the wetting front of the Schirmer strip becomes visible. Details of the initial fast capillary-wetting dynamics do not impact of behavior in the linear length time domain. However, significant evaporation in a low humidity environment does impact wetting kinetics [20,23,25] and abrogates simple assessment of tear production. Clinical evaluation is required to establish the quantitative validity of the proposed methodology.

5. Conclusions

A Schirmer tear test (STT) establishes the sufficiency of human tear production. For insufficient lacrimal supply, dry eye is a possible diagnosis. As practiced, however, a STT reports a wetting length 5 min after strip insertion, not actual tear-production rates. We present a physical model including evaporation and gravity but focusing on wetting dynamics in a Schirmer strip when first inserted into the lower fornix. The strip is treated as a fibrous porous medium that wicks tear at a high rate compared to lacrimal production rate. Accordingly, the strip quickly imbibes tear from the closed-eye tear lake. When tear volume in the lake diminishes to such an extent that the radius of curvature of the arc menisci adjacentto the strip approaches those in the fibrous paper, capillary suction chokes. Tear supply to the Schirmer strip is then furnished only by the lacrimal glands with tear-lake volume remaining static. In comparison to wicking rates, lacrimal supply is slow leading to a slowing of tear penetration along the Schirmer strip. Provided evaporation is minimal, a linear increase in transient wetting length arises when the driving pressure difference per unit wetted-strip length is close to constant. Our proposed physical model explains all reported experimental findings without invoking non-constant lacrimal supply and with no adjustable parameters.

We establish that the linear-length time regime gauges lacrimal supply rates. We suggest a simple extension of current practice in which the Schirmer strip is sheathed against evaporation and the wetted length of a distance-marked strip is measured at three time points near 5 min of insertion. According to Eq. (20), the slope of the resulting best-fit straight line gives basal tear production after a small correction for gravity. The proposed procedure is simple and time efficient. Clinical evaluation is necessary to establish its accuracy and usefulness, especially for distinguishing between evaporative dry eye and aqueous-deficient dry eye [28–30].

Acknowledgment

We thank Andrew Crothers for technical assistance.

Appendix A. Evaluation of evaporation number

Knowledge of the evaporative flux is necessary to ascertain the evaporation number. Thus from Eq. (4), we require the mass transfer coefficient, k_m, and the temperature of the evaporating strip surface, T_S. Energy conservation specifies the strip temperature. As warm tear penetrating the strip emerges from the lower fornix, evaporation into the environment cools the advancing tear [20]. Tear temperature in the strip falls eventually reaching the wet-bulb temperature governed by the expression [15,35–37]

$$\hat{J}_E \Delta\hat{H}_v = h\,[T_\infty - T_S] \qquad \text{(A1)}$$

where $\Delta\hat{H}_v$ is the mass enthalpy of water vaporization (2.453 kJ/g), h is the heat transfer coefficient [15,35,37], and T_∞ is ambient temperature (23 °C). We estimate heat transfer to the Schirmer strip by natural convection at a horizontal planar surface [15,35,37,38]

$$Nu = \frac{hL_c}{k} = 0.96Ra^{1/6} \quad 1 < \mathrm{Ra} < 200$$

where Nu is the Nusselt number, $k[= 2.58x10^{-2}\mathrm{W/m/K}]$ is the thermal conductivity of air, L_c is the characteristic length for evaporation defined as the ratio of the Schirmer-strip surface area to its' perimeter: $L_c = 0.5wL/(w + L)$ with L estimated as an average 10 mm, and Ra is the heat-transfer Rayleigh number defined by

$$Ra = \frac{[\hat{\rho}_a(T_\infty) - \hat{\rho}_a(T_S)]gL_c^3}{\langle\hat{\rho}_a\rangle\nu\alpha} \qquad \text{(A3)}$$

where $\hat{\rho}_a$ is the mass density of humid air, $\langle\hat{\rho}_a\rangle = \left[\hat{\rho}_a(T_\infty) + \hat{\rho}_a(T_S)\right]/2$, $\alpha[= 2.14x10^{-5}\mathrm{m^2/s}]$ is the thermal diffusivity of air, $\nu[= 1.52x10^{-5}\mathrm{m^2/s}]$ is

the kinematic viscosity of air, and g is gravitational acceleration. The mass density of humidified air in Eqn. (A3) is estimated by $\hat{\rho}_a(T)R_G T = M_w R_H P_w^{sat}(T) + M_a[P_{atm} - R_H P_w^{sat}(T)]$ where M_w and M_a are the molar masses of water and dry air, respectively, and P_{atm} is atmospheric pressure. Accordingly, there is a small dependence of Ra, and ipso facto of h and k_m, on environment humidity. Unless otherwise noted, all physical properties are evaluated at the film temperature $T_f = (T_\infty + T_S)/2$. Properties of air are conveniently tabulated in Appendix I of [37]. We obtain $Ra \sim 1.53$ and $h \sim 15.9 \text{W/m}^2\text{/K}$. The mass transfer coefficient of water vapor in air appearing in Eq. (4) must also be calculated to complete assessment of the wet-bulb temperature. Since heat and mass-transfer mechanisms are analogous, the mass transfer coefficient follows Eq. (A2) with the Sherwood number replacing the Nusselt number and the mass-transfer Rayleigh number replacing the heat-transfer Rayleigh number [15,35,37]. Thus, we find that

$$\frac{k_m}{h} = \frac{D_{wa}}{k}\left(\frac{\alpha}{D_{wa}}\right)^{1/6} \qquad \text{(A4)}$$

where D_{wa} [$= 2.56 \times 10^{-5}$ m^2/s] is the molecular diffusion coefficient of water vapor in air. Evaluation of Eqn. (A4) gives $k_m \sim 0.0153$m/s. Given the heat and mass transfer coefficients, Eqs. (4) and (A1) are solved iteratively using a Newton-Raphson algorithm. Resulting wet-bulb temperatures are listed in Table 2 along with $\hat{J}_E$ and E values (based on Q_L = 1 μL/min) at three relative humidities.

References

[1] O. Schirmer, Studien zur physiologie und pathologie der tränenabsonderung und tränenabfuhr, Albr. von Græfe's Arch. für Ophthalmol. 56 (1903) 197–291.

[2] L. Cassen, M. Fingerat, H.T. Woodcome, Atlas of Primary Eye Care Procedures, 2nd ed., McGraw Hill, New York, NY, 1997, Chapter 34.

[3] J.M. Tiffany, N. Winter, G. Bliss, Tear film stability and tear surface tension, Curr. Eye. Res. 8 (1989) 507–515.

[4] N. Ehlers, The precorneal film: biomicroscopical, histological and chemical investigations, Acta Ophthalmol. Suppl. 81 (1965) 1–134.

[5] J.C. Mainstone, A.S. Bruce, T.R. Golding, Tear meniscus measurement in the diagnosis of dry eye, Curr. Eye Res. 15 (1996) 653–661.

[6] S. Mishima, A. Gasset, S.D. Klyce, J.L. Baum, Determination of tear volume and tear flow, Invest. Ophthalmol. Vis. Sci. 5 (1996) 264–276.

[7] C.F. Cerretani, C.J. Radke, Tear dynamics in healthy and dry eyes, Curr. Eye Res. 3683 (2014) 1–16.

[8] F.T. Fraunfelder, Extraocular fluid dynamics − How best to apply topical ocular medication, Trans. Am. Ophthalmol. Soc. 74 (1976) 457–487.

[9] I. Fatt, B.A. Weissman, Physiology of the Eye: An Introduction to the Vegetative Functions, 2nd ed., Butterworth-Heinemann, Boston, MA, 1992, Chapter 10.

[10] M. Conrath, N. Fries, M. Zhang, M.E. Dreyer, Radial capillary transport from an infinite reservoir, Transp. Porous Media 84 (2009) 109–132.

[11] Z. Liu, J. Hu, Y. Zhao, Z. Qu, F. Xu, Experimental and numerical studies on liquid wicking into filter papers for paper-based diagnostics, Appl. Therm. Eng. 88 (2014) 280–287.

[12] H. Hsuan, H.H. Hsu, Particle Movement in Paper Porous Media: Influence Factors and Model Network, 2010 (http://digitalcommons.mcmaster.ca/opendissertations/4509/).

[13] Whatman filter paper #41. http://www.bangkokscience.com/download/bangkokscience com/Whatman%20 Filter%20paper1.pdf.

[14] N. Fries, Capillary Transport Processes in Porous Materials−Experiment and Model, Cuvillier Verlag, Göttingen, 2010.

[15] R.B. Bird, W.E. Stewart, E.N. Lightfoot, Transport Phenomena, 2nd ed., John Wiley and Sons, New York, NY, 2002, Chapter 6,20.

[16] J.C. Wright, G.E. Meger, A review of the Schirmer test for tear production, Arch. Ophthalmol. 67 (1962) 564–565.

[17] S. Vashisht, S. Singh, Evaluation of phenol red thread test versus Schirmer test in dry eyes: a comparative study, Int. J. Appl. Basic Med. Res. 1 (2011) 40–42.

[18] T.E. Clinch, D.A. Benedetto, N.T. Felberg, P.R. Laibson, Schirmer’s test: a closer look, Arch. Ophthalmol. 101 (1983) 1383–1386.

[19] F.J. Holly, D.W. Lamberts, E.D. Esquivel, Kinetics of capillary tear flow in the Schirmer strip, Curr. Eye Res. 2 (1982) 57–70.

[20] F. Buckmaster, E.I. Pearce, Effects of humidity on tests of tear production, 35 2016, 754–758.

[21] G. Savini, P. Prabhawasat, T. Kojima, M. Grueterich, E. Espana, E. Goto, The challenge of dry eye diagnosis, Clin. Ophthalmol. 2 (2008) 31–55.

[22] F.J. Holly, S.J. Laukaitis, E.D. Esquivel, Kinetics of lacrimal secretion in normal human subjects, Curr. Eye Res. 3 (1984) 897–910.

[23] W.E. Beebe, E.D. Esquivel, F.J. Holly, Comparison of lacrimation kinetics in dry eye patients and normal, Curr. Eye Res. 7 (1988) 419–425.

[24] F.J. Holly, Lacrimation kinetics as determined by a Schirmer-type technique, in: D.A. Sullivan (Ed.), In Lacrimal Gland, Tear Film, and Dry Eye Syndromes, Plenum Press, New York, NY, 1994, pp. 543–548.

[25] D.L. Williams, Analysis of tear uptake by the Schirmer tear test strip in the canine eye, Vet. Ophthalmol. 8 (2005) 325–330.

[26] N. Li, X.-G. Deng, M.-F. He, Comparison of the Schirmer I test with and without topical anesthesia for diagnosing dry eye, Int. J. Ophthalmol. 5 (2012) 478–481.

[27] E.M. Hay, E. Thomas, B. Pal, A. Hajeer, H. Chambers, A.J. Silman, Weak association between subjective symptoms or and objective testing for dry eyes and dry mouth: results from a population based study, Ann. Rheum. Dis. 57 (1998) 20–24.

[28] M. Cuevas, M.J. González-García, E. Castellanos, R. Quispaya, P.L. Parra, I. Fernández, M. Calonge, Correlations among symptoms signs, and clinical tests in evaporative-type dry eye disease caused by Meibomian gland dysfunction (MGD), Curr. Eye Res. 37 (2012) 855–863.

[29] B.D. Sullivan, L.A. Crews, E.M. Messmer, G.N. Foulks, K.K. Nichols, P. Baenninger, G. Geerling, F. Figueiredo, M.A. Lemp, Correlations between commonly used objective signs and symptoms for the diagnosis of dry eye disease: clinical implications, Acta Ophthalmol. 92 (2012) 161–166.

[30] K.K. Nichols, J.J. Nichols, G.L. Mitchell, The lack of association between signs and symptoms in patients with dry eye disease, Cornea 23 (2004) 762–770.

[31] E.W. Washburn, The dynamics of capillary flow, Phys. Rev. 17 (1921) 273–283.

[32] V.M. Starov, M.G. Velarde, C.J. Radke, Wetting and Spreading Dynamics, CRC Press, New York, NY, 2007.

[33] J.C. Berg, An Introduction to Interfaces and Colloids: The Bridge to Nanoscience, World Scientific Publishers, Inc, New Jersey, 2016.

[34] P.G. de Gennes, F. Brochard-Wyart, D. Quéré, Capillary and Wetting Phenomena: Drops, Bubbles, Pearls and Waves, Springer Science, New York, NY, 2004.

[35] W.L. McCabe, J.C. Smith, P. Harriot, Unit Operations of Chemical Engineering, 5th ed., McGraw-Hill, New York, NY, 1993, Chapter 7.

[36] C. Cerretani, N. Ho, C.J. Radke, Water-evaporation reduction by duplex films: application to the human tear film, Adv. Coll. Inter. Sci. 197–198 (2013) 33–57.

[37] J.R. Welty, G.L. Rorrer, D.G. Foster, Fundamentals of Momentum, Heat, and Mass Transfer, 6th ed., John Wiley & Sons, New York NY, 2015, Chapter 20.

[38] J.R. Lloyd, W.R. Moran, Natural convection adjacent to horizontal surface of various planforms, J. Heat Trans. 96 (1974) 443–447.